3184–3196 *Nucleic Acids Research, 2019, Vol. 47, No. 6* *Published online 15 January 2019*
doi: 10.1093/nar/gky1324

Reconstitution of the human SRP system and quantitative and systematic analysis of its ribosome interactions

Klemens Wild[1,†], Keven D. Juaire[1,†], Komal Soni[1], Vivekanandan Shanmuganathan[2], Astrid Hendricks[1], Bernd Segnitz[1], Roland Beckmann[2] and Irmgard Sinning[1,*]

[1]Heidelberg University Biochemistry Center (BZH), INF 328, D-69120 Heidelberg, Germany and [2]Gene Center and Center for Integrated Protein Science Munich, Department of Biochemistry, University of Munich, Feodor-Lynen-Str. 25, D-81377 Munich, Germany

Received October 10, 2018; Revised December 20, 2018; Editorial Decision December 28, 2018; Accepted January 02, 2019

ABSTRACT

Co-translational protein targeting to membranes depends on the regulated interaction of two ribonucleoprotein particles (RNPs): the ribosome and the signal recognition particle (SRP). Human SRP is composed of an SRP RNA and six proteins with the SRP GTPase SRP54 forming the targeting complex with the heterodimeric SRP receptor (SRαβ) at the endoplasmic reticulum membrane. While detailed structural and functional data are available especially for the bacterial homologs, the analysis of human SRP was impeded by the unavailability of recombinant SRP. Here, we describe the large-scale production of all human SRP components and the reconstitution of homogeneous SRP and SR complexes. Binding to human ribosomes is determined by microscale thermophoresis for individual components, assembly intermediates and entire SRP, and binding affinities are correlated with structural information available for all ribosomal contacts. We show that SRP RNA does not bind to the ribosome, while SRP binds with nanomolar affinity involving a two-step mechanism of the key-player SRP54. Ultrasensitive binding of SRP68/72 indicates avidity by multiple binding sites that are dominated by the C-terminus of SRP72. Our data extend the experimental basis to understand the mechanistic principles of co-translational targeting in mammals and may guide analyses of complex RNP–RNP interactions in general.

INTRODUCTION

The universally conserved signal recognition particle (SRP) is a prime example for a ribonucleoprotein particle (RNP) with an essential physiological function featuring complex RNA folds and conformational changes, and with the SRP RNA even supporting catalytic activity (1–3). The SRP system is the main targeting route for integral membrane proteins and secretory proteins to the endoplasmic reticulum (ER) in eukaryotes. SRP recognizes hydrophobic N-terminal signal sequences (or signal anchor sequences) of its client proteins as soon as they emerge from the ribosome (4–6). Mammalian SRP comprises the highly base-paired SRP RNA (also referred to as 7SL RNA) of ∼300 nt and six proteins (SRP9, SRP14, SRP19, SRP54, SRP68 and SRP72) (Figure 1A). It is divided into the functionally independent Alu domain (SRP9/14 and 5′/3′ ends of SRP RNA) responsible for translation retardation (7), and the S domain (in the following denoted as SRPS) that recognizes the signal sequence and binds to the membrane-bound SRP receptor (SRαβ heterodimer (8)) in a GTP-dependent manner. The four largest proteins, SRP19, SRP54, SRP68 and SRP72, belong to SRPS and are all essential for SRP function, while the Alu domain is dispensable for protein translocation (9) and the significance of elongation retardation is discussed controversially.

Co-translational targeting is initiated by SRP binding to the ribosome and scanning for nascent chains that carry a signal sequence ('scanning state') prior to the establishment of a committed state when the signal is bound to SRP ('engaged state') in the SRP–RNC pre-handover complex (10–12). Signal sequence recognition correlates with significant structural changes in the key-player SRP54, a multi-domain protein consisting of the signal-binding M (methionine-rich) and the regulatory NG domain (N: four-helix bundle, G: GTPase) (13). The M domain dives into the funnel of the polypeptide tunnel exit of the large ribosomal subunit engaging the signal, while the NG domain is stably locked-in-place across the exit (12,14,15). Upon signal engagement, the SRP–RNC complex is targeted to the ER by interaction

*To whom correspondence should be addressed. Tel: +49 6221 544781; Fax: +49 6221 544790; Email: irmi.sinning@bzh.uni-heidelberg.de
†The authors wish it to be known that, in their opinion, the first two authors should be regarded as Joint First Authors.

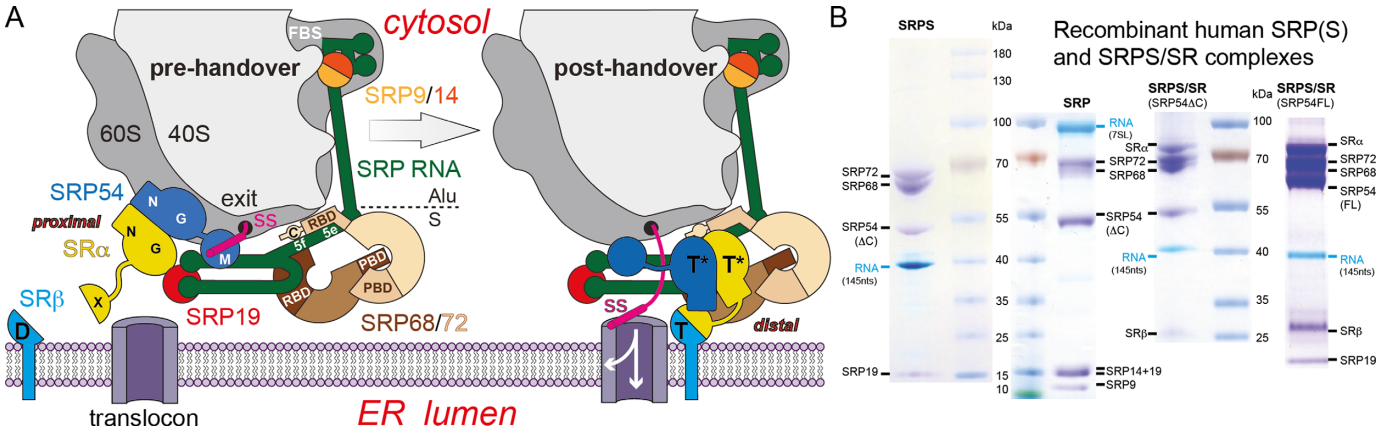

Figure 1. Co-translational targeting by the SRP system. (**A**) Scheme for the mammalian SRP system and the targeting of RNCs to the translocon in the ER membrane. SRP consists of six proteins (numbered by molecular weight in kDa) bound to SRP RNA acting as scaffold. The Alu domain reaches into the factor binding site within the ribosomal 40S/60S subunit interface and the S domain binds to the signal sequence (ss) emerging from the polypeptide exit tunnel (exit) in the signal pre-handover state (left). The multi-domain SRP GTPase SRP54 recognizes the signal with its M domain and establishes the targeting complex consisting of its NG domain bound to the homologous NG domain of the SRP receptor SRα at a proximal ribosome binding site. SRP68/72 are large solenoids including RBD and protein-binding modules. Upon signal handover to the translocon (right), the GTP-dependent (T) stable targeting complex is activated at a distal SRP RNA site (5e and 5f loops; *: activation). The SRX domain of SRα regulates the membrane-anchored Ras-like SRβ GTPase (D: GDP). (**B**) SDS-PAGE gels of fully recombinantly reconstituted and purified SRP/SR complexes (Coomassie and methylene blue stained). SRPS, SRPS/SR and entire SRP can be purified to homogeneity in large scale up to milligram amounts. SRP54 is added either as full-length protein or as C-terminal deletion (ΔC) lacking the flexible signal-enclosing and exit-binding region.

with the SRP receptor (SR), and the RNC is finally handed-over to a vacant translocation channel (translocon, Sec61 complex) (Figure 1A).

The targeting complex (TC) formed by the SRP GTPases SRP54 and SRα constitutes the core of the SRP system and regulates the entire process (16–19). The TC forms close to the ribosomal tunnel exit at the 'proximal site' of the SRP RNA and is relocated to a conserved 'distal site' in the middle of the SRP RNA after the signal sequence is handed over to the translocon. Only then, the SRP GTPases are stimulated by the RNA as validated for bacteria (18). After initially observing the removal of the TC from the proximal binding site (20), the distal binding of the TC has recently been visualized by high-resolution cryo-EM for the mammalian system (18,21). GTP-hydrolysis dissociates SRP from the SR, translation resumes, and the targeting cycle is completed.

Most of the structural and biochemical studies have been performed for the bacterial system from Gram-negative *Escherichia coli* as it only consists of the SRP GTPases Ffh and FtsY bound to the single stem–loop SRP RNA of 114 nt (4.5S RNA). The bacterial system is easy to reconstitute as the RNA folds intrinsically and Ffh binds to the RNA on its own (22). Furthermore, GTP-hydrolysis by the two SRP GTPases can be readily measured by fluorescence methods (23) and by using the NG domain of FtsY without the intrinsically disordered N-terminal A domain. In contrast, due to its complexity the mammalian SRP system imposes several obstacles that need to be overcome. Typically, mammalian SRP has been purified from microsomes derived from canine pancreatic tissue (24). Thus, amounts were limited and although the particle can be disassembled and functionally reconstituted (25), the material was not suited for biochemical or biophysical assays affording highly pure and/or modifiable components. In order to overcome this drawback, we set up a large-scale reconstitution and purification protocol for the entire SRP, the SRPS domain (sufficient for fully active translocation (9)) and the heterodimeric SR (without N-terminal TMD, dispensable for function (26)). While a parallel study used the reconstitution of mammalian SRP for a mainly kinetic description (21,27), we employed the reconstitution of the SRP system in a comprehensive, quantitative study of its ribosome interactions by microscale thermophoresis (MST). The protocols developed here are valuable tools for other ribosome associated complexes and for analyzing the interactions of hitherto less characterized RNPs.

MATERIALS AND METHODS

In the following, we focus on the description of reconstitution and purification of the human SRP system and the details of MST as key-method applied in this study. All materials and methods (including buffer composition) regarding RNA and protein production as well as on the purification of human 80S ribosomes and rabbit reticulocyte RNCs are described in detail in the online Supplementary Data.

SRP(S) and SRP(S)/SR complex formation and purification

Complex formation and purification have been successively established and refined over the years starting from small SRPS RNA/SRP19 binary complexes (28) up to finally the entire SRP system. The protein components were individually purified as monomers or respective heterodimers for SRP9/14, SRP68/72 and SRαβ. Potential trimming of flexible termini was based on stability tests and crystal structure analyses of all components. Protein concentrations were measured either at 280 nm if purity was high (> 95%) or by Bradford assay and corrected according to the relative purity estimated from quantitative analysis of sodium dodecyl

sulphate-polyacrylamide gel electrophoresis (SDS-PAGE) lanes.

For complex formation, each RNA construct was pre-assayed for optimal folding by native RNA-PAGE analysis in a Tris/$Mg(OAc)_2$ buffer system. Briefly, RNAs were either folded via a rapid snap-cooling from 90°C in ice water (SRPS RNA with 145 nt: 105–249) or slow-cooled from 65 to 25°C (7SL RNA) in Buffer C. The snap-cooled RNA was supplemented with Buffer C lacking NaCl and incubated for 5 min at 37°C.

SRP and SR proteins were then subsequently added either as monomers or as preformed heterodimers (9/14, 68/72 and SRαβ) and incubated at room temperature in slightly super-stoichiometric amounts with increasing excess from 120% to 200% for at least 5 min per addition. The hierarchy of protein addition always starts with the scaffolding protein SRP19 (together with SRP9/14 for the entire SRP) followed by SRP68/72 and finally by SRP54. The SRP receptor was then added and the mixture incubated for 10 min at 37°C with an excess (2 mM) of non-hydrolyzable GTP analog (GMP-PNP: 5′-guanylyl-imidodiphosphate). After a short resting phase on ice, the sample was centrifuged for 10 min at 14 000 × g to remove potential aggregates. All assembled complexes were immediately purified via size-exclusion chromatography (SEC) in Buffer L containing 20 mM 4-(2-hydroxyethyl)-1-piperazineethanesulfonic acid (HEPES; pH 7.5), 250 mM KOAc, 5 mM $Mg(OAc)_2$ and 1 mM Tris(2-carboxyethyl)phosphine hydrochloride (TCEP). Thus, all assemblies with ribosomal samples were done in homogeneous buffer compositions. Respective SEC fractions of the SRP/SR complexes were pooled and immediately concentrated in a centrifugal filter device (Millipore). The overall yield of complex formation was usually in the range from 5% to 25%.

Microscale thermophoresis

In the MST setup, a dilution series of a ligand is mixed with a low 'tracer' concentration of a fluorophore-labeled target. The mixtures are filled in glass capillaries and placed on a temperature-controlled sample tray that is excited with an LED light and locally heated with an infrared laser (29). The change of fluorescence upon heating mainly due to thermophoresis (MST amplitude) is then recorded and data points are presented in a dose–response curve. For MST measurements, human 80S ribosomes or rabbit reticulocyte RNCs were labeled with Atto-647 NHS-ester dye (N-HydroxySuccinimide, Thermo Fisher). For this purpose, the Atto-dye stock (2 mM in dimethyl sulfoxide (DMSO)) was diluted to a final concentration of 50 μM in Buffer Q. Equal volumes of sample (100 μl, 100–500 nM) and dye solution were mixed and the labeling reaction was incubated for 30 min at RT in the dark. The excess dye was removed from the sample by purification over a desalting column (Zeba Spin, Thermo Fisher) equilibrated with Buffer Q. A degree of labeling (DOL) of ∼4–8 dye molecules per ribosome was determined by absorption measurements. As for the RNCs, partial labeling of the nascent chain cannot be excluded. However, due to the low DOL and randomness of labeling we assume the effective ribosome concentrations in the MST calculations to be close to the measured concentrations and labeling generally not to interfere with the binding events. The concentrations of the labeled ribosomes were adjusted to 1 to 20 nM (1 OD_{260} = 20 nM) depending on the estimated strength of the interaction to be measured (see Supplementary Table S1 for all parameters in the respective experiments). For K_D measurements according to the law of mass action, fluorophore concentrations need to be lower than the K_D-value, but due to sensitivity limitations in the experimental setup, concentrations below 1 nM were not possible. All SRP/SR ligands were carefully diluted in 16 micro reaction tubes in Buffer L (16× serial 1:1 dilution, final volume of 10 μl each) with concentrations between 100 μM and 5 pM with the highest concentration adapted to the strength of the interaction (usually at least 20× the K_D-value). SRP/SR samples and ribosomes (10 μl each) were then mixed in a 1:1 ratio (final K^+ concentration of 175 mM approximating physiological conditions) and incubated at RT for 10 min before being loaded into 16 premium coated glass capillaries (NanoTemper Technologies).

MST measurements were performed using a Monolith NT.115 (NanoTemper Technologies) according to manufacturer's instructions (LED red). MST measurements were carried out at 20°C with LED powers ranging from 60 to 100% according to the input concentration of the fluorophore. Each measurement was typically done at three infrared-laser (MST) powers between 40% and 100%. One measurement was defined by measuring the initial fluorescence signal for 5 s (baseline) followed by MST for 30 s (fluorescence changes due to thermophoresis) and finishing by again determining the fluorescence signal for 5 s (reverse thermophoresis due to back diffusion upon cooling). The obtained data were analyzed assuming a 1:1 binding model and by using the MO.Affinity Analysis Software (NanoTemper Technologies) at the default time windows (violet bars: baseline; red bars: used MST signals). Data from at least three independent measurements were combined to create one dataset for which the averaged data points were fitted using a K_D-model (for K_D-values > fluorophore concentration). For independent and non-cooperative two-site binding data (SRP54), analysis was done with program PALMIST (30).

For K_D-values lower than or equal to the fluorophore concentration, accurate values cannot be obtained and titrations result in dose–response curves yielding EC50-values that are best fitted with a Hill-model (29). In these cases, the K_D-values can be estimated to be lower than the determined EC50-values. In case of K_D-values being significantly lower than the fluorophore concentration, saturation curves with a kink at the point of saturation are obtained that allow for the determination of the interaction stoichiometry at the concentration of saturation. For ultra-sensitive binding events, where the fluorescence change is significantly steeper than for simple 1:1 binding and where K_D-values are higher than the fluorophore concentration (SRP72), EC50-values determined via the Hill-model give an approximation for the K_D-values. Here, binding induces cooperativity (Hill coefficient > 1), which indicates the involvement of multiple dependent binding sites and might reflect conformational changes within the ligand upon bind-

ing (31). Thus, ultrasensitivity can be described as single avidity process with multiple and synergistic affinities.

RESULTS

Large-scale reconstitution of the human SRP system

The production of recombinant RNPs critically depends on the folding of the RNA scaffold (32). Each individual RNP and RNA construct requires careful adaptation of the protocol for RNA folding. In contrast to *E. coli* SRP with its plain stem–loop 4.5S RNA, mammalian SRP RNA (7SL RNA) needs a temperature step for folding. For SRPS RNA (145 nts), we found that it folds best via fast snap-cooling in water before the addition of magnesium and potassium ions. In contrast, folding of the entire SRP RNA was optimized by a slow-cooling procedure in a folding buffer additionally containing sodium chloride.

RNP assembly *in vivo* is generally performed in a hierarchical fashion to ensure correct maturation of the particle (33). In our *in vitro* assembly scheme, SRP and SR proteins were thus added in a defined order either as monomers or as preformed heterodimers (9/14, 68/72 and SRαβ) and incubated at room temperature in slightly super-stoichiometric amounts with increasing excess from 120% to 200% (Supplementary Figure S1). SRP assembly intermediates were analyzed by electrophoretic mobility shift assays and purified by size-exclusion chromatography to homogeneity up to milligram amounts (Figure 1B and Supplementary Figures S2 and S3). The order of protein addition starts with the scaffolding protein SRP19 (together with SRP9/14 for entire SRP) followed by the RNA modifiers SRP68/72 (or their RNA binding domains, RBDs). SRPS is stepwise assembled from sub-complexes starting from SRP RNA/SRP19 (binary complex), SRP RNA/SRP19/SRP54 (ternary complex), SRP RNA/SRP19/SRP68/72 (quaternary complex) and the entire SRPS with all four proteins. Only in the presence of SRP19, SRP RNA is folded with an exposed binding platform that allows SRP54 incorporation into the particle reflecting the *in vivo* situation (34) and as analyzed in detail before (35–37).

The SRP receptor was subsequently added at 37°C with an excess of a non-hydrolyzable GTP analog (GMP-PNP: 5′-guanylyl-imidodiphosphate) either as SRαNG domain only, as full-length protein including the N-terminal X domain (38) or as deletion construct lacking the charged ribosome-binding region (RBR) in the X-NG linker (39). The small Arf-like integral membrane GTPase SRβ that binds the X domain was co-expressed in solution without its N-terminal TMD to form a GTP-stable SRαβ complex (40). Incubation of SRPS with the SR results in the reconstitution of the stable SRPS/SR targeting complex, which does not require the Alu domain.

In order to obtain systematic quantitative data of the human co-translational targeting system, we aimed at the reconstitution of a complete homologous system including human ribosomes. Large-scale preparations for Puromycin-treated human monosomes from HeLa cells had been established for previous structural studies (41,42). We adapted the protocols for buffer homogeneity and speed to maintain the vulnerable RNA expansion segments of the human ribosome. The homogeneity and quality of the human monosomes were assessed by negative-stain and high-resolution single particle cryo-EM at 3.3 Å. The tunnel exit, and therefore the SRPS/SR binding site, was found to be protein free.

Thermodynamic dissection of SRP interactions with the ribosome

MST is a recently established method to determine accurate dissociation constants (K_D-values) in the picomolar to millimolar range within minutes with almost no restriction to molecular mass and low sample requirements (29). It is thus perfectly suited to study large molecular assemblies like the SRP/SR/ribosome system. MST measures concentration variations of an intrinsically or labeled fluorescent probe in a temperature gradient. Here, the ribosomes were covalently labeled with an N-HydroxySuccinimide-ester (NHS-ester) absorbing at 647 nm. The fluorescence signal allowed for measurements of the labeled ribosomes at concentrations between 1 and 20 nM with a typical value of approximately 10 nM ($OD_{260} = 0.5$) resulting in signal amplitudes of normalized fluorescence between 30 and 1300. Subsequently we tested all individual components, different mutant variants as well as sub-complexes, and entire SRPS or SRP(S)/SR assemblies for their affinities with the human ribosome and integrated the data in the known structural and functional context.

First, SRP RNA alone does not interact at all with the ribosome (Figure 2A and Supplementary Figure S4A). Further, neither SRP19 nor the binary SRPS complex (SRP RNA/SRP19) bind, which confirms previous SRP/ribosome cryo-EM structures showing SRP19 not to be in direct contact with the ribosome (12,14). To test for the significance of our S-domain binding data, we added the Alu domain to the binary complex by including the entire 7SL RNA of 300 nt and the SRP9/14 heterodimer. Indeed, also this complex is unable to bind to ribosomes demonstrating that the Alu domain does not significantly contribute to ribosome binding.

Next, we tested various constructs of SRP68/72, which are known to remodel the SRP RNA (43). We first used the C-terminal region of SRP72 including the RBD (SRP72-RBD+C) that binds to SRP RNA and constitutes the major part of a contact between SRP and the ribosome observed by cryo-EM ('C4-contact' (11,44)). This SRP72 variant alone binds to the ribosome with a K_D-value of roughly 1 μM (920 ± 150 nM) (Figure 2B), showing that even in the absence of SRP RNA and despite the intrinsic flexibility of SRP72–RBD (44) the ribosome-binding epitope is formed. We further examined whether SRP72 has additional binding sites with the ribosome. Fitting the SRP72 data to a simple K_D-model results in an unaltered affinity (820 ± 320 nM) (Supplementary Figure S5). However, the steepness of the curve is indicative of an ultrasensitive binding event resembling cooperativity ($n = 2.8$), and data fit substantially better to a Hill-model resulting in an increased affinity (520 ± 40 nM) (Figure 2B and Supplementary Figure S5). In order to see whether the SRP68 subunit of the physiological heterodimer modifies the affinity, we added full-length SRP68 in a SRP68/72 complex. Indeed, the complete heterodimer binds about three times stronger with an affinity of 160 ± 20 nM and with similar ultrasensitivity ($n = 2.3$) that

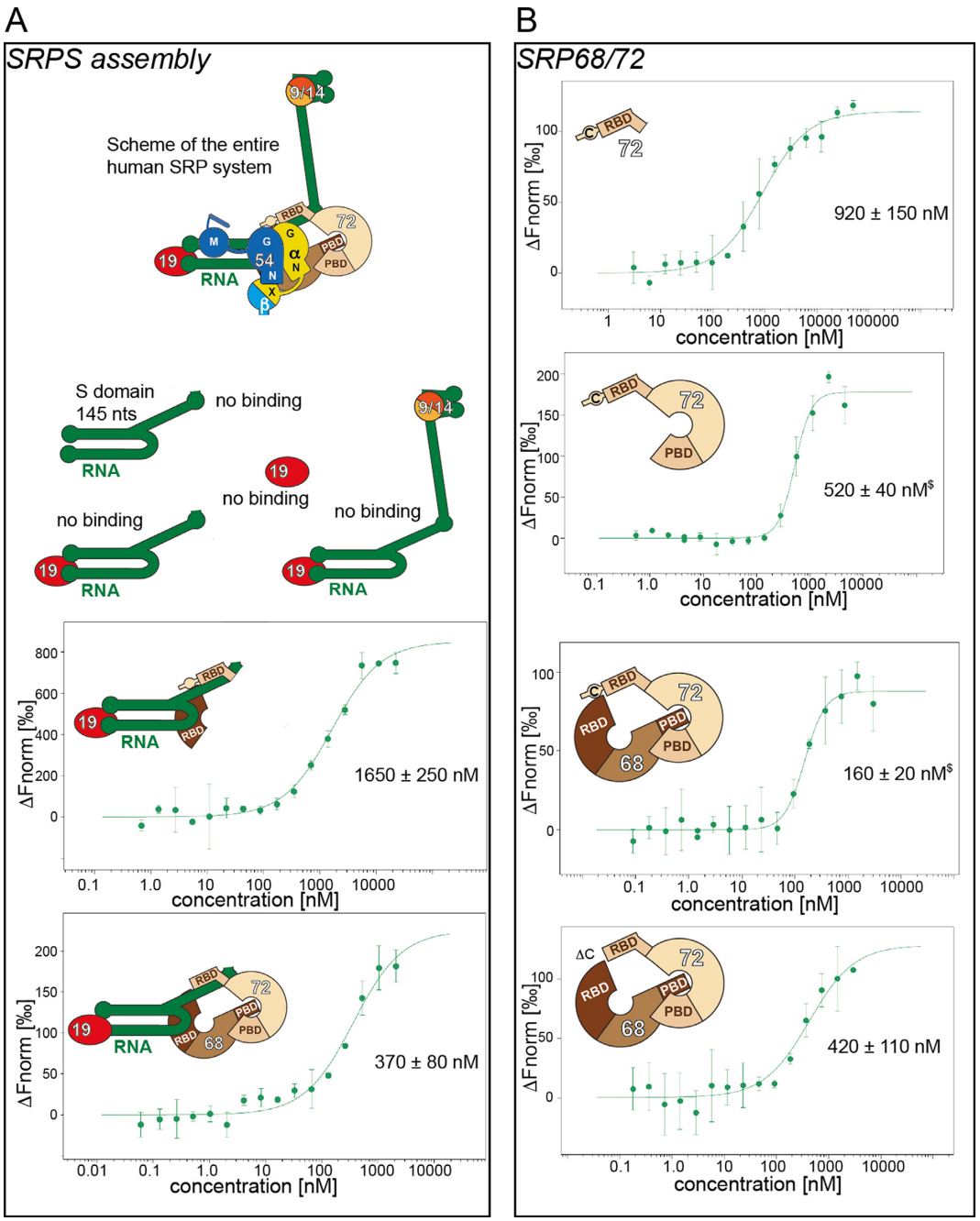

Figure 2. MST data for SRPS assembly complexes and SRP68/72 with the 80S ribosome. (**A**) SRPS assembly: SRP RNA, SRP19 and the binary complex thereof do not bind to the ribosome. The Alu domain including the SRP9/14 heterodimer is not a primary ribosomal-binding site. Low affinity SRPS binding to the ribosome is induced by the SRP68/72 heterodimer. The interaction involves more than the SRP68/72 RBD-domains previously characterized as ribosome binders at the C4-contact. (**B**) SRP68/72: Ribosome binding of heterodimer constructs. SRP72–RBD alone binds weakly and the large solenoidal parts of SRP68/72 contribute significantly. The flexible very C-terminus of SRP72 is relevant for ribosome binding. $^{\$}$: Binding of SRP72 is ultrasensitive (Hill-model with EC50 values), indicative for multiple binding sites and an avidity mechanism.

therefore can be attributed to SRP72. Previously, we identified a surface loop of SRP68 interacting with 28S rRNA at the C4-contact (44). However, it seems unlikely that this small contact site alone accounts for the observed stronger binding observed for the heterodimer. If we truncate the C-terminus of SRP72 (last 70 residues) to the structured region of SRP72–RBD as seen in our recent crystal structure (44), the affinity of this SRP68/72 variant drops to 420 ± 110 nM. In this case, ultrasensitivity is weaker and the binding curve can be approximated by a simple K_D-model. These data show that the very C-terminus, a region physiologically and pathologically relevant due to phosphorylation and caspase cleavage (45), contributes significantly to ribosome binding.

We next added the SRP68/72 heterodimer to the binary SRPS complex to form a quaternary SRPS

(RNA/SRP19/68/72) complex. This assembly intermediate constitutes the nucleolar pre-SRPS (the Alu domain folds independently) prior to the final SRP54 addition in the cytosol (34). We started with the truncated SRP68/72–RBD constructs as previously published (44). Interestingly, this complex (including the SRP72 C-terminus) binds with slightly lower affinity to the ribosome (1.65 ± 0.25 μM) (Figure 2A) compared to SRP72-RBD+C alone (1 μM), indicating a repulsion of the SRP RNA in this sub-complex missing the major part of SRP68/72. When we employ the SRP68/72 heterodimer (without the SRP72 C-terminus), we find again a significant increase in ribosome binding (K_D of 370 ± 80 nM, in range with isolated SRP68/72ΔC), supporting the observation that a major contribution to SRPS–ribosome interaction stems from the large solenoidal parts of SRP68/72. In line with this finding, mutation of the SRP RNA at the 5f-loop within the C4-contact (44) (231-AG to 231-GA) are not sufficient to significantly impair SRP-ribosome binding (data not shown).

Taken together our data show that binding of the SRP68/72 heterodimer follows an ultrasensitive response dependent on the SRP72 C-terminus. Although the large solenoids of SRP68/72 have not been structurally characterized due to intrinsic flexibility, they serve as important contact sites in ribosome interaction.

SRP54 is the major determinant of SRP–ribosome interaction

In order to complete SRPS assembly, we investigated the contribution of SRP54 to ribosome binding. SRP54 is a multi-domain protein (NGM domains) with the C-terminal M domain being responsible for SRP RNA, signal sequence and ribosome binding at the polypeptide tunnel exit of the 60S ribosomal subunit. We started the MST analyses with full-length SRP54 and ribosomes (Figure 3A). Full-length SRP54 alone already binds with high affinity (K_D1 of 30 ± 10 nM, sub-curve fitting in the nanomolar range). However, the data cannot be fitted at micromolar concentrations due to aggregation effects, which is a known phenomenon of SRP54M that complements its hydrophobic binding site *in trans* (46). When the SRP54 C-terminus is truncated to the well-structured SRP54M domain by deleting 70 residues (SRP54ΔC), the stability of the protein is significantly increased. The binding curve of SRP54ΔC reveals two inflection points suggesting a two-site binding mode (30) with an overall K_D of ∼200 nM (Figures 3A and 4). While the first binding event clearly shows a K_D ∼ 100 nM, an additional low affinity interaction is detected in the micromolar range. To dissect this bimodal binding, we measured affinities for SRP54MΔC and SRP54NG individually. Indeed, the separate titrations coincide with a high affinity for SRP54MΔC (K_D1 of 100 ± 20 nM) and a low affinity binding for SRP54NG (K_D2 of 1.65 ± 0.45 μM) (Figure 4).

When we replace human SRP54 for the bacterial homolog Ffh from *E. coli*, which can functionally replace SRP54 in *in vitro* translocation assays (47) but lacks the extended C-terminus, we find an ∼10-fold reduction in the overall affinity (2.30 ± 0.6 μM) (Figure 3A). Chloroplast SRP54 from *Arabidopsis thaliana,* which acts both in a co- and post-translational mode, contains an even further extended C-terminus involved in *cp*SRP43 protein binding (48,49). However, despite the extension that is enriched in positively charged residues (50), cpSRP54 shows low affinity binding to human ribosomes with a K_D in the low micromolar range (>1.2 μM, not fitted to saturation due to aggregation, cp. human SRP54). These data highlight species-specific differences in the interaction between SRP54 and the tunnel exit.

With the assembly of a ternary SRPS complex consisting of SRP RNA/SRP19/54, we observe a further increase in ribosome binding affinity (K_D-value < 4.7 nM) compared to SRP54 alone (Figure 3B). This high affinity pushes the analysis toward its limits as the fluorophore (ribosomes at 4.7 nM) is present in the same concentration range as the K_D-value and thus an accurate value cannot be given. Here it does not matter, whether we use the SRP54ΔC construct or full-length SRP54. Due to the tight binding, we almost obtain a saturation curve indicated by an emerging 'kink' upon saturation. Saturation occurring around the fluorophore concentration additionally allows for the validation of the 1:1 stoichiometry of our SRP systems bound to ribosomes.

When we now form complete SRPS including all four SRP S domain proteins, we measure the same high affinity in saturation with K_D's below 4.7 nM for particles including either SRP54 or SRP54ΔC (Figure 3C). Especially for the complex with full-length SRP54, the saturation curve is shifted toward lower concentrations indicating enhanced binding in respect to SRP54ΔC. The data reveal stronger binding than observed by previous fluorescence-based binding measurements in equilibrium using either native SRP from pancreatic tissue and non-translating wheat-germ ribosomes (K_D of 71 nM, (51)) or MST using reconstituted human SRP and rabbit-reticulocyte ribosomes (K_D of 120 nM, (27)) and validate the high quality of our *in vitro* reconstituted SRP complexes.

SRP consists of two functional folding units, namely SRPS and the Alu domain. In order to validate our different reconstituted SRPS complexes as the main ribosome-binding domains, we reconstituted the entire human SRP consisting of the native 7SL RNA and all six SRP proteins (Figure 1B and Supplementary Figure S1). Folding of 7SL RNA is significantly more difficult than for SRPS RNA and slow-cooling is superior to snap-cooling. Nevertheless, complete recombinant human SRP can be purified using the assembly scheme established for SRPS. The MST measurements revealed high affinity binding of SRP to ribosomes in the (sub-) nanomolar range (saturation well below the used ribosome concentration of 2.2 nM) similar to SRPS alone (Figure 5A). The Alu domain might slightly contribute to ribosome binding, which however cannot be quantified with the current setup.

The modulation of SRP-ribosome interaction by SR

In the next step, we included the SRP receptor, which is known to be involved in ribosome binding (15,38,52). Recently, we found that a conserved and positively charged ribosome-binding region (RBR) in the linker between the X and NG domains of SRα is responsible for SRαβ affinity for the ribosome as demonstrated by pull-down assays (39).

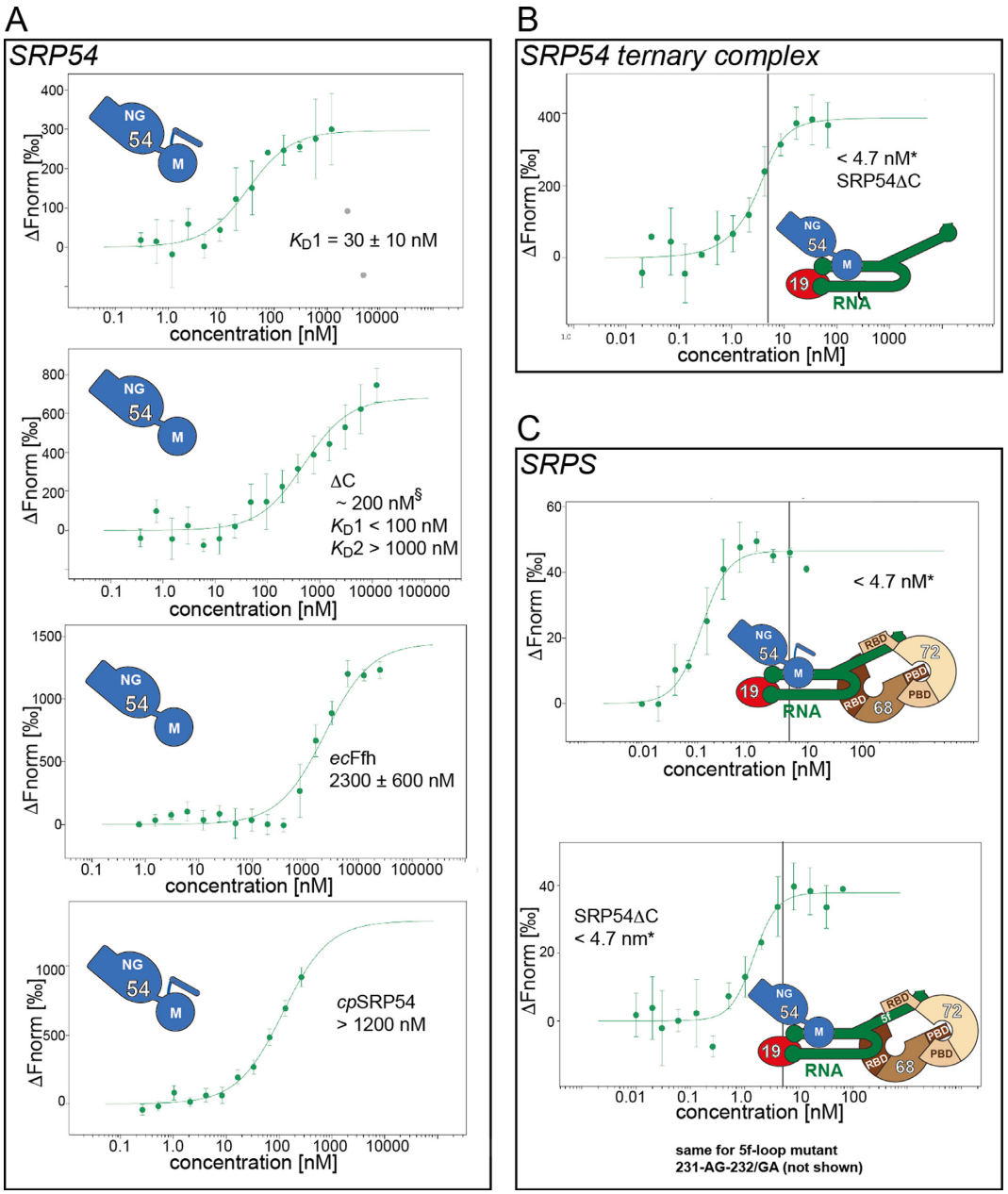

Figure 3. MST data for SRP54 proteins and SRPS complexes. (**A**) SRP54: The conserved SRP key-player binds with high affinity (K_D1) to the ribosome. MST data at higher concentration show aggregation (gray dots). The binding curve for the stable SRP54ΔC construct, missing a flexible C-terminus adjusting between ribosome and signal sequences, is double-sigmoidal and reveals a high (K_D1) and low (K_D2) affinity binding event (§: overall affinity). Homologous SRP54 proteins from bacteria (*Escherichia coli*) and chloroplasts (*Arabidopsis thaliana*) show a significantly reduced affinity to human ribosomes. (**B**) SRPS ternary complex: SRP54 assembly into the binary SRP RNA/SRP19 complex results in high affinity binding of the ternary complex. Binding of SRP54 is almost saturated (saturation curves are indicated with an asterisk) at used ribosome concentrations (given as vertical line), and K_D-values can only be estimated to be at lower concentrations. A Hill-model is used to optimally fit the saturation curve. (**C**) SRPS complexes: Ribosome binding of entire SRPS occurs way below the ribosome concentrations for both SRP54 and its truncated construct SRP54ΔC and saturation (kinking of the curve) is more pronounced.

Using the MST setup as above, we obtain a K_D-value of 410 ± 50 nM for the SRαβ heterodimer (Figure 5B, upper panels), which is higher than reported earlier by biosensor techniques (52). When we delete the entire N-terminal region of SRα including the linker and the X domain (and therefore SRβ), this SRαNG construct is unable to bind to the ribosome, thus confirming the importance of the N-terminal binding epitope. Moreover, when we perform our measurements with a SRαΔRBR/SRβ construct, we hardly observe any binding (K_D > 7.5 μM), which is consistent with previous pull-down data (39).

Finally, we employ all components in the assembly of the entire human SRP(S)/SR/ribosome system. Assaying SRPS/SR without signal sequence in MST, we obtain K_D-values in the (sub-)nanomolar range (<1.4 nM with SRP54 and <1.2 nM with SRP54ΔC, respectively) thereby bring-

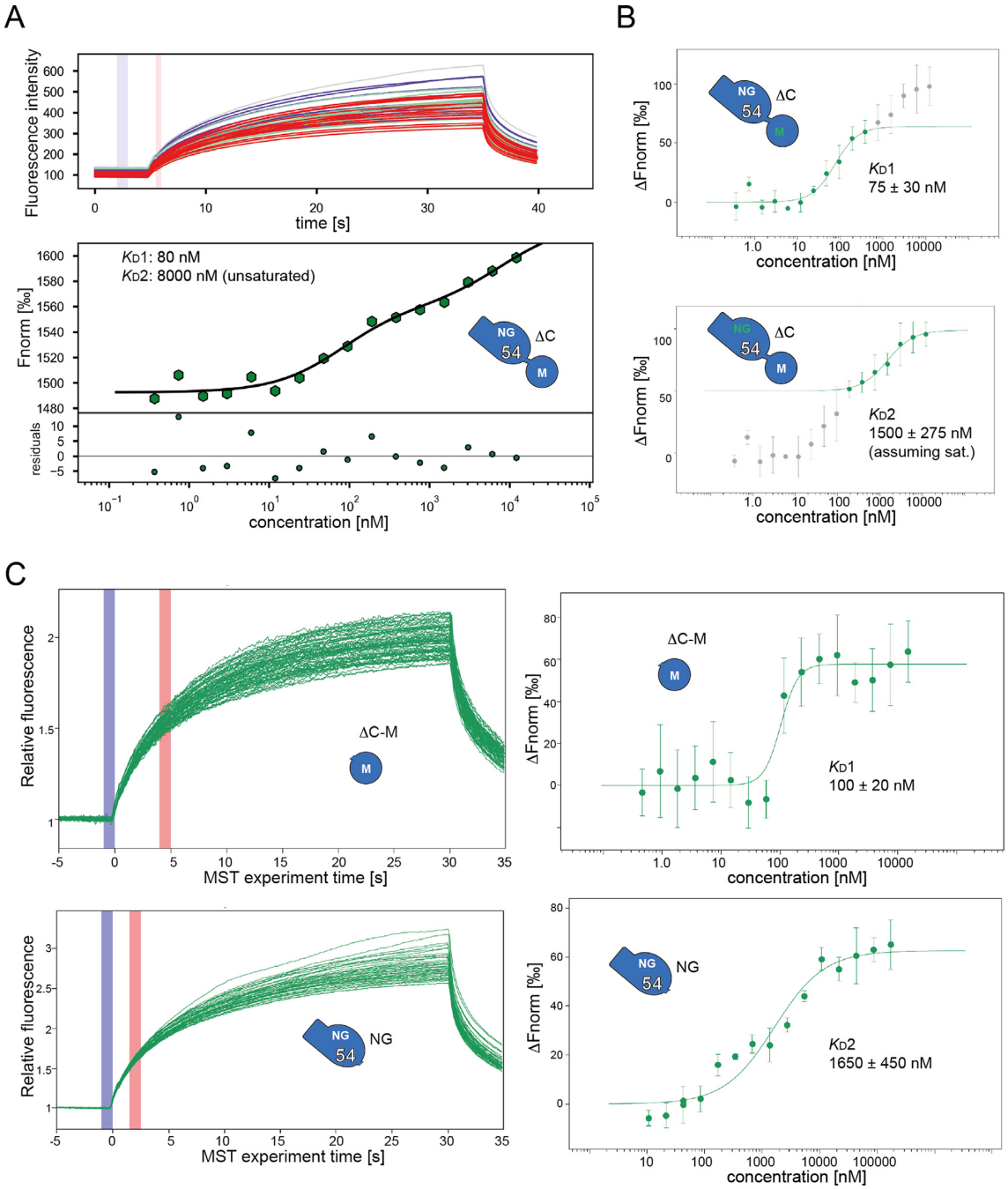

Figure 4. High and low affinity binding of SRP54 domains with the ribosome. (**A**) Two-site binding analysis of the SRP54ΔC–ribosome interaction using program PALMIST (30) (upper panel: fluorescence intensity data, lower panel: two-site fitted relative fluorescence with residuals). High affinity binding (K_D1) occurs below 100 nM, while low affinity is in the micromolar range (K_D2) and does not reach complete saturation. (**B**) Split sub-curve single binding event analyses using the single-site analysis software (MO.Affinity). Top: High affinity binding yields a value of roughly 75 nM and might correspond to M-domain binding. Bottom: Fitting of the high concentration data confirms the low micromolar affinity. Note: Data evaluation is performed at the same (early, 5 s) time windows for both types of analyses. (**C**) MST measurements of SRP54 domains. Upper panels: Raw MST data and binding curve for SRP54MΔC. The domain binds with high affinity with a K_D of 100 nM (K_D1). Lower panels: SRP54NG binds in the micromolar range (K_D2) as estimated from the SRP54ΔC measurement. Notes: (i) MST data for highest concentrations of SRP54NG and at late MST times show aggregation effects. (ii) A putative two-site binding of SRP54NG is not evaluated.

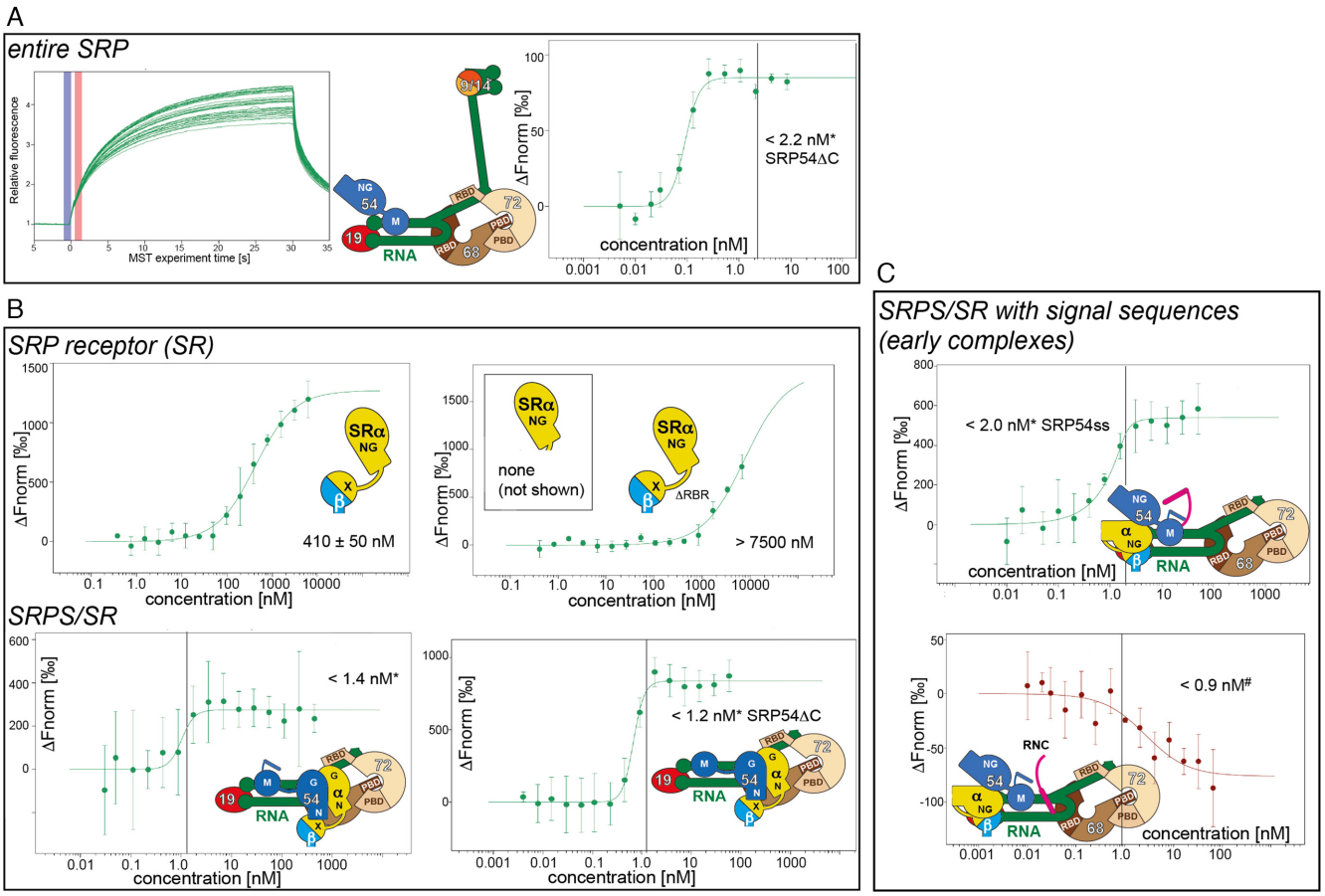

Figure 5. MST data for entire SRP and SRP receptor complexes with and without signal. (**A**) Entire SRP: Fully assembled recombinant SRP binds with high affinity in the low nanomolar range to empty human ribosomes (Hill-fitted saturation curve). The original MST trace is shown as typical example, highlighting the data quality even at lowest fluorophore concentrations. (**B**) SRP receptor (SR) and SRPS/SR complexes: The SRαβ heterodimer binds to the ribosome by itself with high affinity. Interaction occurs via a positively charged RBR in the X-NG linker of SRα. All SRPS/SR complexes bind to the ribosome in the sub-nanomolar range. (**C**) SRPS/SR with signal sequences: SRPS/SR with SRP54 fused to a signal sequence binds at least as good as without signal (sharp kink in saturation curve). Ribosome binding using RNCs with a stalled translation and exposing an SRP substrate occurs with sub-nanomolar affinity and validates the MST setup. Due to the pre-handover state (bound signal before translocon docking), the TC is drawn at the proximal site of the SRP RNA. #: The RNCs (rabbit reticulocyte lysate ribosomes) behave differently in the MST measurements (highlighted in red).

ing our MST measurements to the limits of detection (Figure 5B, lower panels). In presence of the receptor, SRP binding to the ribosome is increased, although it is not known whether this reflects the direct binding of SR to the ribosome according to a dual recognition (52) or is due to other stabilizing effects. Inline with these observations, a strong influence of the ribosome on the SRP/SR interaction has been recently described for the mammalian system (27).

Contribution of the signal sequence

In order to simulate binding of a nascent chain in the SRP–RNC pre-handover state, we fused a typical signal sequence (ss, from yeast dipeptidyl aminopeptidase B) to the C-terminus of full-length SRP54 (SRP54ss), an approach that has been validated previously (53). This SRP54 variant alone binds to the ribosome with an overall K_D of ∼200 nM (Supplementary Figure S4B). SRP54ss shows similar stability as SRP54ΔC (see above) and does not aggregate due to hydrophobic interactions like full-length SRP54. As expected, incorporating the signal into SRPS using SRP54ss results in a very strong binding (<2.0 nM for SRPS/SR) as observed for SRP without signal (Figure 5C).

In order to complete the MST study with the physiologically relevant SRPS/SR/RNC interaction, we measured the affinity of the entire recombinant SRPS/SR system to RNCs exposing an SRP-targeting signal. While the thermophoretic behavior is different for the rabbit reticulocyte-lysate RNCs compared to the non-translating human ribosomes, we again observe a very high binding affinity with a K_D in the sub-nanomolar range (<0.9 nM) (Figure 5C). Using our experimental setup, we thus cannot differentiate between the affinities of SRP and SRP/SR for empty ribosomes and those exposing a nascent chain. However, similar values have been reported recently also from MST experiments using reconstituted human SRP with a fused signal sequence (5.1 ± 2 nM) or with an RNC carrying a signal sequence (3.1 ± 1 nM) (27). Therefore, having a signal sequence fused to SRP54 or presented by the ribosome does not seem to significantly change SRP binding to the ribosome.

In summary, the values as obtained here by all MST analyses give a comprehensive survey of the strength of the interactions between human ribosomes (or RNCs) with the co-translational protein targeting machinery including both SRP and SR, and pinpoint the individual contributions of each component, which match current structural and functional data.

DISCUSSION

While co-translational targeting by the SRP system is universally conserved, its complexity evolved simultaneously with the diversification of life. Mammalian SRP and SR involve eight proteins acting at the ER membrane. We established the recombinant purification of all components and the stepwise reconstitution of various sub-complexes finally resulting in the complete reconstitution of the mammalian SRP system. All SRP complexes can be formed and purified to homogeneity, and their ribosome interactions were analyzed guided by high-resolution structural data from X-ray crystallography and cryo-EM.

With all human components on hand, we started the dissection of the interaction of SRP/SR with the ribosome and RNCs, respectively. We established the individual contributions of single components, sub-domains or mutant variants, and of constitutive heterodimers on ribosome binding affinity (K_D-values) by MST. MST analyses using labeled ribosomes instead of various labeled ligands guarantee a consistent setup for all affinity measurements. Moreover, comparative experiments by fluorescence anisotropy fail under these conditions, and classical isothermal titration calorimetry is unfeasible in terms of quantity and concentrations necessary. The obtained quantitative MST data are in excellent agreement with the contacts visualized by the currently available cryo-EM data, schematized in Figure 6, using native SRP derived from pancreatic tissue. Nearly, all MST data have been acquired with highly purified non-translating human ribosomes reflecting a scanning mode of SRP/SR (and especially SRP54) for a client protein bearing a signal sequence. Intriguingly, SRP amounts in mammalian cells are estimated to be 10–100 times (∼500 nM (54)) lower than ribosomes, and fast scanning is necessary for efficient protein targeting (55).

As revealed by our MST data, SRP RNA alone does not bind to the ribosome, which might reflect the lack of a stable 3D-fold when not bound to any SRP protein (36,56). However, even the reconstitution with SRP19 (to fold the S domain RNA) or with SRP9/14 (to fold the Alu domain) does not induce ribosome binding, showing that RNA folding per se is not sufficient. When we follow the *in vivo* SRP assembly path, which as ribosome biogenesis takes place in the nucleolus, and only add the SRP68/72 RBDs and the C-terminus of SRP72 to the folded S domain RNA alongside SRP19, we observe a first weak ribosome binding. With the addition of the complete SRP68/72 heterodimer binding affinity increases significantly, showing that SRPS variants are sufficient for ribosome interaction. Thus, the Alu domain does not significantly contribute to binding, which agrees with previous data indicating that SRP in the scanning mode is able to stay bound to translating ribosomes and the Alu domain may still be detached (12).

Despite the recent progress in the biochemical and structural characterization of crucial parts of the eukaryote-specific SRP68/72 heterodimer (43,44), its entire structure and function have not been elucidated. The stepwise analyses of these two large solenoidal proteins in our study confirm the significance of the ribosomal C4-contact (11,44). However, our data show that in particular the unstructured C-terminus of SRP72, which is physiologically important and involved in regulation (45), is also an important determinant of ribosome interaction and seems to cause an ultrasensitive binding response. Ultrasensitivity in binding, also known as avidity (31) observed i.e. in simultaneous antibody–antigen interactions (57), indicates multiple binding sites within SRP72 to the ribosome. All current cryo-EM structures of mammalian SRP at the ribosome suffer from SRP dynamics, resulting in a dramatic difference in resolution between the ribosome (<3.5 Å) and different parts of SRP (ranging from 4 to 15 Å or being completely disordered) (12,21,58). So far, only a small part of the SRP68/72 heterodimer has been resolved on the ribosome (with rather low local resolution), while the major part of both solenoidal proteins is obviously too dynamic. Similarly, in mammals the ribosomal RNA contains large expansion segments, some of them (ES27L and ES39L) in close vicinity of SRP68/72, which are also not resolved in the cryo-EM structures and might at least transiently contact the heterodimer. It seems, that the entire SRP72-RBD+C region first needs to be stably engaged with the ribosome to allow subsequent interactions likely induced by conformational changes within SRP68/72.

Similarly, the ribosomal-binding sites of SR are changing during the SRP cycle and have not been pinpointed, although they were validated by cross-linking and various biochemical and biophysical assays (15,38,39,52). Recently, we identified the flexible and highly positively charged RBR within the X-NG linker of SRα as a main contributor to the interaction (39), which nicely matches our MST data. The interaction of similar RBR regions present in protein linkers or tails is an emerging theme in a multitude of dynamic complexes of associated factors with ribosomes such as chloroplast cpSRP54, co-translational chaperones like the Hsp70 Ssb (59) or the nascent polypeptide-associated complex (NAC) (60), or the evolutionary conserved YidC/Oxa1/Alb3 receptor family (61). Given the recent advances in cryo-EM technology, high-resolution structure determination of these complexes becomes feasible.

The multi-domain SRP54 protein undergoes the largest conformational changes within SRP, and mediates and regulates all states along the SRP cycle. For SRP54, we were able to discriminate two binding events manifested in a two-site binding curve. The distinction of two events requires independent binding with significantly different affinities (30) in contrast to the cooperative ultrasensitive interaction as observed for SRP72. While the molecular interpretation of such events is not straightforward, the comparison of MST data for the entire protein and its single domains allows for the assignment of the binding events to individual domain interactions with the ribosome. The M and NG domains are known to be uncoupled by a flexible linker helix making an independent binding highly plausible (11–13).

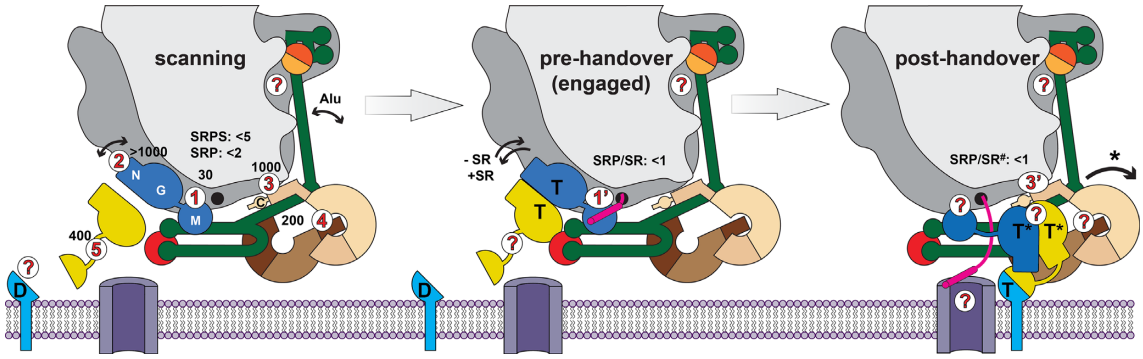

Figure 6. Scheme of SRP/SR/ribosome interactions in the SRP cycle. Left panel: SRP(S) strongly binds to the ribosome in the scanning state (individual contributions in nM determined by MST are discerned). SRP54 reveals a dual binding mode by its M (high affinity (1)) and NG domains (low affinity (2)). Contributions of the Alu domain and SRβ are not defined. SRP68/72 interactions (4) are ultrasensitive, include more than the C4-contact (3) established by SRP72–RBD, and involve the C-terminus (C). Middle panel: in the pre-handover state (engaged) interactions are reinforced mainly by signal sequence recognition of SRP54M (1′) and SRP54NG is locked in place (12,14). Upon SR binding, ribosome affinity is as strong although the TC complex of the NG domains is known to dissociate from the ribosome (20). Right panel: Upon translocon docking, the TC relocates and the signal is handed-over. No structure of any post-handover complex is available and individual contributions are elusive. TC re-localization induces a rotation of SRPS in respect to the ribosome and a modification of the C4-contact (3′) at the distal site (20,44). Only upon GTP-hydrolysis, SRP dissociates from the ribosome (indicated by asterisks) and the SRP cycle is completed. #: MST data for SRPS/SR indicate a very tight RNC interaction before GTP-hydrolysis occurs (although the Alu domain and translocon were missing in the assay).

As inferred from cryo-EM data, the first and high-affinity binding reflects the tight contact of the M domain at the ribosomal tunnel exit, while the second and weaker contact corresponds to the NG domain when it binds across the exit in the scanning and the engaged pre-handover states (10,11). Our MST data also highlight the importance of the C-terminus of SRP54M in ribosome binding. The tail including two amphipathic helices is known to fold into the signal-binding groove of SRP54M in the absence of the signal and to form a lid in its presence (12,58) thus completing the groove to form a hydrophobic barrel. Our MST data show, that SRP54 binding by itself is rather strong with a K_D-value of 30 nM that weakens about threefold upon deletion of the SRP54M C-terminus. The weak binding of SRP54NG in the low micromolar range nicely matches with the rather small interface between SRP54N and the ribosomal proteins uL23 and uL29 across the tunnel exit shown in cryo-EM structures (12,58).

Furthermore, comparison of MST data from human SRP54 with bacterial Ffh and chloroplast *cp*SRP54 reveals that despite the high conservation of the ancient SRP54 protein family (19), this key subunit has undergone specific adaptations to match the ribosomal surface of the respective organism. Of note, the SRP54 homolog Ffh from *E. coli* does not contain the extended C-terminus (47 residues shorter), but binds only slightly weaker (∼80 and 1 nM for RNCs (62)) than reported for mammalian SRP (∼71 nm and 0.2 nM for wheat-germ RNCs (51)), and the SRP-ribosome interaction in *E. coli* occurs nearly exclusively via the Ffh M domain (63). Specific adaptations are also observed at the ribosome around the tunnel exit e.g. the bacterial extensions of ribosomal proteins uL23 or the chloroplast specific extension of uL24c and uL29c (64). These extensions seem even more important considering that in the chloroplasts of higher plants (like *A. thaliana*) *cp*SRP54 acts on its own in the co-translational mode as *cp*SRP has lost the SRP RNA (65). These data highlight the importance of using a homologous system for quantitative studies.

Our MST data of SRPS complexes show that as long as SRP54 is not assembled into SRP, ribosome binding is of moderate affinity at most. Eukaryotic SRP assembly *in vivo* proceeds in the nucleolus until all protein components are incorporated except for SRP54, which is added in the cytosol (34,66). The details of SRP biogenesis are not known, however separating it in two parts, a nucleolar and a cytosolic one, is essential for correct SRP assembly (67). This ensures that only upon addition of SRP54, SRP will bind efficiently to ribosomes (100× increased affinity with SRP54), which excludes non-functional particles (without SRP54) from competing for ribosome binding. Given the importance of the SRP pathway for protein targeting, it seems unlikely that the biogenesis of SRP is unmonitored. Whether there are quality control mechanisms in the nucleolus that prohibit the export of incomplete or damaged SRP assembly intermediates is not known. In eukaryotic ribosome biogenesis, more than 200 protein factors are necessary to drive and control the assembly and maturation of the two ribosomal subunits (68). When pre-60S is exported to the cytosol, the ribosomal tunnel exit is occupied by late biogenesis factors that need to be removed before the 60S is ready to engage in translation (69). Excluding SRP54 from the nucleus is an elegant way to avoid premature completion of SRP, which otherwise might interfere with maturation of the pre-60S particle.

In order to answer specific biochemical and functional questions of SRP/ribosome interactions, the complete *in vitro* reconstitution of the SRP system as described here is required. The quality of the recombinant particles is validated by high affinity binding to the ribosome in the low nanomolar or (as for the RNC) even sub-nanomolar range as measured by MST. MST is thus a valuable tool to complement modern RNP biology as performed by high-throughput or single-molecule methods. The MST values obtained here for non-translating ribosomes are at least 50 times stronger than reported previously for the eukaryotic SRP system (27,51), which we attribute to the enhanced pu-

rity and the use of an entirely human system. As the concentration of ribosomes in the cell is in the micromolar range, a thermodynamic control of co-translational targeting is impossible and would sequester most of SRP in unproductive complexes. The high affinity of SRP throughout the SRP cycle shown here supports the idea that faithful co-translational protein targeting is rather a question of binding kinetics (3,70), creating a time window for conformational changes of the targeting machinery in respect to the ribosome. Overall, our study provides valuable tools and protocols for the *in vitro* analysis of SRP/ribosome interaction and may serve as an example for the analysis of complex RNP–RNP interactions in general.

SUPPLEMENTARY DATA

Supplementary Data are available at NAR Online.

ACKNOWLEDGEMENTS

We acknowledge help in negative-stain and cryo-EM data acquisition and processing by Dirk Flemming and Stefan Pfeffer. We thank Pauline Heckmann and Michelle Haas for assistance in sample preparation and help in MST measurements. We are grateful for advice in MST analysis by Tobias Pflüger. Irmgard Sinning is an investigator of the Cluster of Excellence:CellNetworks.

FUNDING

DFG through the Leibniz programme (to I.S.); DFG fellowship through the Graduate School of Quantitative Biosciences Munich (QBM) (to V.S). Funding for open access charge: Leibniz Programme.
Conflict of interest statement. None declared.

REFERENCES

1. Elvekrog,M.M. and Walter,P. (2015) Dynamics of co-translational protein targeting. *Curr. Opin. Chem. Biol.*, **29**, 79–86.
2. Grudnik,P., Bange,G. and Sinning,I. (2009) Protein targeting by the signal recognition particle. *Biol. Chem.*, **390**, 775–782.
3. Zhang,X. and Shan,S.O. (2014) Fidelity of cotranslational protein targeting by the signal recognition particle. *Annu. Rev. Biophys.*, **43**, 381–408.
4. Schibich,D., Gloge,F., Pohner,I., Bjorkholm,P., Wade,R.C., von Heijne,G., Bukau,B. and Kramer,G. (2016) Global profiling of SRP interaction with nascent polypeptides. *Nature*, **536**, 219–223.
5. Noriega,T.R., Chen,J., Walter,P. and Puglisi,J.D. (2014) Real-time observation of signal recognition particle binding to actively translating ribosomes. *Elife*, **3**, doi:10.7554/eLife.04418.
6. Walter,P. and Blobel,G. (1981) Translocation of proteins across the endoplasmic reticulum. II. Signal recognition protein (SRP) mediates the selective binding to microsomal membranes of in-vitro-assembled polysomes synthesizing secretory protein. *J. Cell Biol.*, **91**, 551–556.
7. Siegel,V. and Walter,P. (1988) Each of the activities of signal recognition particle (SRP) is contained within a distinct domain: analysis of biochemical mutants of SRP. *Cell*, **52**, 39–49.
8. Tajima,S., Lauffer,L., Rath,V.L. and Walter,P. (1986) The signal recognition particle receptor is a complex that contains two distinct polypeptide chains. *J. Cell Biol.*, **103**, 1167–1178.
9. Siegel,V. and Walter,P. (1986) Removal of the Alu structural domain from signal recognition particle leaves its protein translocation activity intact. *Nature*, **320**, 81–84.
10. Wild,K., Halic,M., Sinning,I. and Beckmann,R. (2004) SRP meets the ribosome. *Nat. Struct. Mol. Biol.*, **11**, 1049–1053.
11. Halic,M. and Beckmann,R. (2005) The signal recognition particle and its interactions during protein targeting. *Curr. Opin. Struct. Biol.*, **15**, 116–125.
12. Voorhees,R.M. and Hegde,R.S. (2015) Structures of the scanning and engaged states of the mammalian SRP-ribosome complex. *Elife*, **4**, doi:10.7554/eLife.07975.
13. Rosendal,K.R., Wild,K., Montoya,G. and Sinning,I. (2003) Crystal structure of the complete core of archaeal signal recognition particle and implications for interdomain communication. *Proc. Natl. Acad. Sci. U.S.A.*, **100**, 14701–14706.
14. Halic,M., Becker,T., Pool,M.R., Spahn,C.M., Grassucci,R.A., Frank,J. and Beckmann,R. (2004) Structure of the signal recognition particle interacting with the elongation-arrested ribosome. *Nature*, **427**, 808–814.
15. Pool,M.R., Stumm,J., Fulga,T.A., Sinning,I. and Dobberstein,B. (2002) Distinct modes of signal recognition particle interaction with the ribosome. *Science*, **297**, 1345–1348.
16. Egea,P.F., Shan,S.O., Napetschnig,J., Savage,D.F., Walter,P. and Stroud,R.M. (2004) Substrate twinning activates the signal recognition particle and its receptor. *Nature*, **427**, 215–221.
17. Focia,P.J., Shepotinovskaya,I.V., Seidler,J.A. and Freymann,D.M. (2004) Heterodimeric GTPase core of the SRP targeting complex. *Science*, **303**, 373–377.
18. Shen,K., Arslan,S., Akopian,D., Ha,T. and Shan,S.O. (2012) Activated GTPase movement on an RNA scaffold drives co-translational protein targeting. *Nature*, **492**, 271–275.
19. Wild,K., Bange,G., Motiejunas,D., Kribelbauer,J., Hendricks,A., Segnitz,B., Wade,R.C. and Sinning,I. (2016) Structural basis for conserved regulation and adaptation of the signal recognition particle targeting complex. *J. Mol. Biol.*, **428**, 2880–2897.
20. Halic,M., Gartmann,M., Schlenker,O., Mielke,T., Pool,M.R., Sinning,I. and Beckmann,R. (2006) Signal recognition particle receptor exposes the ribosomal translocon binding site. *Science*, **312**, 745–747.
21. Kobayashi,K., Jomaa,A., Lee,J.H., Chandrasekar,S., Boehringer,D., Shan,S.O. and Ban,N. (2018) Structure of a prehandover mammalian ribosomal SRP.SRP receptor targeting complex. *Science*, **360**, 323–327.
22. Voigts-Hoffmann,F., Schmitz,N., Shen,K., Shan,S.O., Ataide,S.F. and Ban,N. (2013) The structural basis of FtsY recruitment and GTPase activation by SRP RNA. *Mol. Cell*, **52**, 643–654.
23. Shen,K., Wang,Y., Hwang Fu,Y.H., Zhang,Q., Feigon,J. and Shan,S.O. (2013) Molecular mechanism of GTPase activation at the signal recognition particle (SRP) RNA distal end. *J. Biol. Chem.*, **288**, 36385–36397.
24. Walter,P. and Blobel,G. (1983) Signal recognition particle: a ribonucleoprotein required for cotranslational translocation of proteins, isolation and properties. *Methods Enzymol.*, **96**, 682–691.
25. Walter,P. and Blobel,G. (1983) Disassembly and reconstitution of signal recognition particle. *Cell*, **34**, 525–533.
26. Ogg,S.C., Barz,W.P. and Walter,P. (1998) A functional GTPase domain, but not its transmembrane domain, is required for function of the SRP receptor beta-subunit. *J. Cell Biol.*, **142**, 341–354.
27. Lee,J.H., Chandrasekar,S., Chung,S., Hwang Fu,Y.H., Liu,D., Weiss,S. and Shan,S.O. (2018) Sequential activation of human signal recognition particle by the ribosome and signal sequence drives efficient protein targeting. *Proc. Natl. Acad. Sci. U.S.A.*, **115**, E5487–E5496.
28. Wild,K., Sinning,I. and Cusack,S. (2001) Crystal structure of an early protein-RNA assembly complex of the signal recognition particle. *Science*, **294**, 598–601.
29. Seidel,S.A., Dijkman,P.M., Lea,W.A., van den Bogaart,G., Jerabek-Willemsen,M., Lazic,A., Joseph,J.S., Srinivasan,P., Baaske,P., Simeonov,A. *et al.* (2013) Microscale thermophoresis quantifies biomolecular interactions under previously challenging conditions. *Methods*, **59**, 301–315.
30. Tso,S.C., Chen,Q., Vishnivetskiy,S.A., Gurevich,V.V., Iverson,T.M. and Brautigam,C.A. (2018) Using two-site binding models to analyze microscale thermophoresis data. *Anal. Biochem.*, **540–541**, 64–75.
31. Kitov,P.I. and Bundle,D.R. (2003) On the nature of the multivalency effect: a thermodynamic model. *J. Am. Chem. Soc.*, **125**, 16271–16284.
32. Edelmann,F.T., Niedner,A. and Niessing,D. (2014) Production of pure and functional RNA for in vitro reconstitution experiments. *Methods*, **65**, 333–341.

33. Oeffinger,M. and Montpetit,B. (2015) Emerging properties of nuclear RNP biogenesis and export. *Curr. Opin. Cell Biol.*, **34**, 46–53.
34. Politz,J.C., Yarovoi,S., Kilroy,S.M., Gowda,K., Zwieb,C. and Pederson,T. (2000) Signal recognition particle components in the nucleolus. *Proc. Natl. Acad. Sci. U.S.A.*, **97**, 55–60.
35. Maity,T.S. and Weeks,K.M. (2007) A threefold RNA-protein interface in the signal recognition particle gates native complex assembly. *J. Mol. Biol.*, **369**, 512–524.
36. Wild,K., Bange,G., Bozkurt,G., Segnitz,B., Hendricks,A. and Sinning,I. (2010) Structural insights into the assembly of the human and archaeal signal recognition particles. *Acta Crystallogr. D Biol. Crystallogr.*, **66**, 295–303.
37. Kuglstatter,A., Oubridge,C. and Nagai,K. (2002) Induced structural changes of 7SL RNA during the assembly of human signal recognition particle. *Nat. Struct. Biol.*, **9**, 740–744.
38. Fulga,T.A., Sinning,I., Dobberstein,B. and Pool,M.R. (2001) SRbeta coordinates signal sequence release from SRP with ribosome binding to the translocon. *EMBO J.*, **20**, 2338–2347.
39. Jadhav,B., McKenna,M., Johnson,N., High,S., Sinning,I. and Pool,M.R. (2015) Mammalian SRP receptor switches the Sec61 translocase from Sec62 to SRP-dependent translocation. *Nat. Commun.*, **6**, 10133.
40. Schlenker,O., Hendricks,A., Sinning,I. and Wild,K. (2006) The structure of the mammalian signal recognition particle (SRP) receptor as prototype for the interaction of small GTPases with Longin domains. *J. Biol. Chem.*, **281**, 8898–8906.
41. Khatter,H., Myasnikov,A.G., Natchiar,S.K. and Klaholz,B.P. (2015) Structure of the human 80S ribosome. *Nature*, **520**, 640–645.
42. Khatter,H., Myasnikov,A.G., Mastio,L., Billas,I.M., Birck,C., Stella,S. and Klaholz,B.P. (2014) Purification, characterization and crystallization of the human 80S ribosome. *Nucleic Acids Res.*, **42**, e49.
43. Grotwinkel,J.T., Wild,K., Segnitz,B. and Sinning,I. (2014) SRP RNA remodeling by SRP68 explains its role in protein translocation. *Science*, **344**, 101–104.
44. Becker,M.M., Lapouge,K., Segnitz,B., Wild,K. and Sinning,I. (2017) Structures of human SRP72 complexes provide insights into SRP RNA remodeling and ribosome interaction. *Nucleic Acids Res.*, **45**, 470–481.
45. Utz,P.J., Hottelet,M., Le,T.M., Kim,S.J., Geiger,M.E., van Venrooij,W.J. and Anderson,P. (1998) The 72-kDa component of signal recognition particle is cleaved during apoptosis. *J. Biol. Chem.*, **273**, 35362–35370.
46. Keenan,R.J., Freymann,D.M., Walter,P. and Stroud,R.M. (1998) Crystal structure of the signal sequence binding subunit of the signal recognition particle. *Cell*, **94**, 181–191.
47. Powers,T. and Walter,P. (1997) Co-translational protein targeting catalyzed by the Escherichia coli signal recognition particle and its receptor. *EMBO J.*, **16**, 4880–4886.
48. Holdermann,I., Meyer,N.H., Round,A., Wild,K., Sattler,M. and Sinning,I. (2012) Chromodomains read the arginine code of post-translational targeting. *Nat. Struct. Mol. Biol.*, **19**, 260–263.
49. Stengel,K.F., Holdermann,I., Cain,P., Robinson,C., Wild,K. and Sinning,I. (2008) Structural basis for specific substrate recognition by the chloroplast signal recognition particle protein cpSRP43. *Science*, **321**, 253–256.
50. Groves,M.R., Mant,A., Kuhn,A., Koch,J., Dubel,S., Robinson,C. and Sinning,I. (2001) Functional characterization of recombinant chloroplast signal recognition particle. *J. Biol. Chem.*, **276**, 27778–27786.
51. Flanagan,J.J., Chen,J.C., Miao,Y., Shao,Y., Lin,J., Bock,P.E. and Johnson,A.E. (2003) Signal recognition particle binds to ribosome-bound signal sequences with fluorescence-detected subnanomolar affinity that does not diminish as the nascent chain lengthens. *J. Biol. Chem.*, **278**, 18628–18637.
52. Mandon,E.C., Jiang,Y. and Gilmore,R. (2003) Dual recognition of the ribosome and the signal recognition particle by the SRP receptor during protein targeting to the endoplasmic reticulum. *J. Cell Biol.*, **162**, 575–585.
53. Janda,C.Y., Li,J., Oubridge,C., Hernandez,H., Robinson,C.V. and Nagai,K. (2010) Recognition of a signal peptide by the signal recognition particle. *Nature*, **465**, 507–510.
54. Kulak,N.A., Pichler,G., Paron,I., Nagaraj,N. and Mann,M. (2014) Minimal, encapsulated proteomic-sample processing applied to copy-number estimation in eukaryotic cells. *Nat. Methods*, **11**, 319–324.
55. Ogg,S.C. and Walter,P. (1995) SRP samples nascent chains for the presence of signal sequences by interacting with ribosomes at a discrete step during translation elongation. *Cell*, **81**, 1075–1084.
56. Menichelli,E., Isel,C., Oubridge,C. and Nagai,K. (2007) Protein-induced conformational changes of RNA during the assembly of human signal recognition particle. *J. Mol. Biol.*, **367**, 187–203.
57. Rudnick,S.I. and Adams,G.P. (2009) Affinity and avidity in antibody-based tumor targeting. *Cancer Biother. Radiopharm.*, **24**, 155–161.
58. Halic,M., Blau,M., Becker,T., Mielke,T., Pool,M.R., Wild,K., Sinning,I. and Beckmann,R. (2006) Following the signal sequence from ribosomal tunnel exit to signal recognition particle. *Nature*, **444**, 507–511.
59. Gumiero,A., Conz,C., Gese,G.V., Zhang,Y., Weyer,F.A., Lapouge,K., Kappes,J., von Plehwe,U., Schermann,G., Fitzke,E. *et al.* (2016) Interaction of the cotranslational Hsp70 Ssb with ribosomal proteins and rRNA depends on its lid domain. *Nat. Commun.*, **7**, 13563.
60. Wegrzyn,R.D., Hofmann,D., Merz,F., Nikolay,R., Rauch,T., Graf,C. and Deuerling,E. (2006) A conserved motif is prerequisite for the interaction of NAC with ribosomal protein L23 and nascent chains. *J. Biol. Chem.*, **281**, 2847–2857.
61. Seitl,I., Wickles,S., Beckmann,R., Kuhn,A. and Kiefer,D. (2014) The C-terminal regions of YidC from Rhodopirellula baltica and Oceanicaulis alexandrii bind to ribosomes and partially substitute for SRP receptor function in Escherichia coli. *Mol. Microbiol.*, **91**, 408–421.
62. Bornemann,T., Jockel,J., Rodnina,M.V. and Wintermeyer,W. (2008) Signal sequence-independent membrane targeting of ribosomes containing short nascent peptides within the exit tunnel. *Nat. Struct. Mol. Biol.*, **15**, 494–499.
63. Jomaa,A., Boehringer,D., Leibundgut,M. and Ban,N. (2016) Structures of the E. coli translating ribosome with SRP and its receptor and with the translocon. *Nat. Commun.*, **7**, 10471.
64. Bieri,P., Leibundgut,M., Saurer,M., Boehringer,D. and Ban,N. (2017) The complete structure of the chloroplast 70S ribosome in complex with translation factor pY. *EMBO J*, **36**, 475–486.
65. Ziehe,D., Dunschede,B. and Schunemann,D. (2017) From bacteria to chloroplasts: evolution of the chloroplast SRP system. *Biol. Chem.*, **398**, 653–661.
66. Grosshans,H., Deinert,K., Hurt,E. and Simos,G. (2001) Biogenesis of the signal recognition particle (SRP) involves import of SRP proteins into the nucleolus, assembly with the SRP-RNA, and Xpo1p-mediated export. *J. Cell Biol.*, **153**, 745–762.
67. Maity,T.S., Leonard,C.W., Rose,M.A., Fried,H.M. and Weeks,K.M. (2006) Compartmentalization directs assembly of the signal recognition particle. *Biochemistry*, **45**, 14955–14964.
68. Woolford,J.L. Jr. and Baserga,S.J. (2013) Ribosome biogenesis in the yeast Saccharomyces cerevisiae. *Genetics*, **195**, 643–681.
69. Kater,L., Thoms,M., Barrio-Garcia,C., Cheng,J., Ismail,S., Ahmed,Y.L., Bange,G., Kressler,D., Berninghausen,O., Sinning,I. *et al.* (2017) Visualizing the Assembly Pathway of Nucleolar Pre-60S Ribosomes. *Cell*, **171**, 1599–1610.
70. Holtkamp,W., Lee,S., Bornemann,T., Senyushkina,T., Rodnina,M.V. and Wintermeyer,W. (2012) Dynamic switch of the signal recognition particle from scanning to targeting. *Nat. Struct. Mol. Biol.*, **19**, 1332–1337.